Computational Modeling of a Smart Impeller actuated by Shape Memory Alloys

Kazeem O. Sanusi, *Member, IAENG*, Olukayode L. Ayodele, Godwin Fuhnwi

***Abstract*— This paper demonstrates numerical investigations using analytical algorithms and advanced computer simulation package to study the performance of a pumping system and the best angle of attack for a Shape Memory Impeller. Comparing the analytical algorithm and simulation, it shows that the best angle of attack is 12 degree at the outlet angle with respect to the inlet angle. Increasing the angle of attack from 35 degree to 45 degree at the outlet there is huge increase in flow rate by 63.47% and slight decrease in the impeller Torque from 35 degrees to 42 degrees by 0.72%. This study successfully conceptualised a Shape Memory Smart Centrifugal Impeller that will increase fluid flow rate through a given system if the fluid temperature increases above a given transition temperature using NiTi Shape Memory Alloys was achieved.**

***Index Terms*— Smart; shape memory alloy; pumps; impeller; Angle of attack; EFD; Nickel-Titanium**

I. Introduction

In recent years, convectional structures are being converged to smart structures by introducing smart material. Smart materials are normally composed of group 4-12 elements, also called transition elements. Compounds formed by transition elements use to have unique behaviour, they tends to behave strange way in response to external environmental changes, like pressure, temperature etc [1]. Shape memory alloys (SMA's) are novel materials which have the ability to return to a predetermined shape when heated [2, 3]. When this material is cold, or below its transformation temperature, it has a very low yield strength and can be deformed quite easily into any new shape which it will retain and it heated above its transformation temperature, it undergoes a change in crystal structure which causes it to return to its original shape [4, 5] (see Figure1). If SMA encounters any resistance during this transformation, it can generate extremely large forces. This phenomenon provides unique mechanisms for remote actuation [6]. Shape memory alloys such as Nickel-Titanium (NiTi) are distinguished by two unusual characteristics, i.e. the shape memory effect and pseudo-elasticity [7, 8]. Pseudo elasticity refers to the material's ability to be strained significantly and return to its unstrained configuration upon loading via a hysteresis loop [9, 10, 11]. A diffusionless transformation between two solid state metallurgical phases called Austenite and Martensite is responsible for both effects and can be induced by either changes in stress or temperature [10]. NiTi shape memory metal alloy can exist in a two different temperature-dependent crystal structures (phases) called martensite (lower temperature) and austenite (higher temperature or parent phase). Several properties of austenite NiTi and martensite NiTi are notably different [12].When martensite NiTi is heated, it begins to change into austenite (Figure 3A). The temperature at which this phenomenon starts is called austenite start temperature (A_s). The temperature at which this transformation is complete is called austenite finish temperature (A_f). When austenite NiTi is cooled, it begins to transform into martensite. The temperature at which this transformation starts is called martensite start temperature (M_s). The temperature at which martensite is again completely reverted is called martensite finish temperature (M_f) [10, 13] . Composition and metallurgical treatments have dramatic impacts on the above transition temperatures. From the point of view of practical applications, NiTi can have three different forms: martensite (at temperatures below A_s), stress-induced martensite (at temperatures above A_f), and austenite (at temperatures above A_f). When the material is in its martensite form, it is soft and ductile and can be easily deformed. Super elastic NiTi is highly elastic (rubber-like), while austenitic NiTi is quite strong and hard (similar to titanium) (Figure 3B).

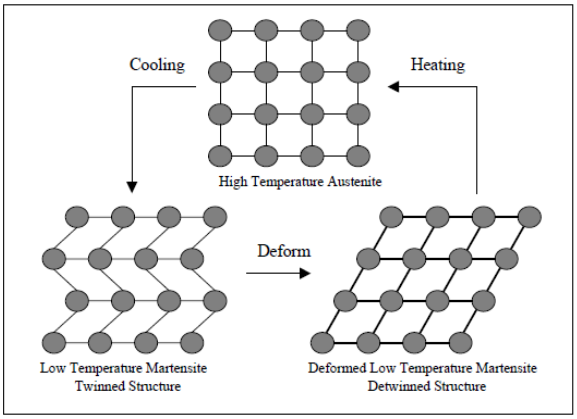

Figure 1: SMA microstructural behaviour.

Manuscript received February 29, 2016; revised July XX, 20XX.. This work was supported by the National Research Foundation (NRF), South Africa.

K. O. Sanusi, is with the Faculty of Engineering and the Built Environment, Department of Mechanical Engineering Science, University of Johannesburg, Auckland Park Kingsway Campus, Johannesburg 2028, South Africa corresponding author phone: +27832071016; e-mail: sanusik@gmail.com

Olukayode L. Ayodele is with the Faculty of Engineering, Department of Mechanical Engineering, Cape Peninsula University of Technology, Cape Town, South Africa; corresponding author phone: +27820925793 E mail. ayodeleo@cput.ac.za

Godwin fuhnwi is with the Eskom , Johannesburg, , South Africa

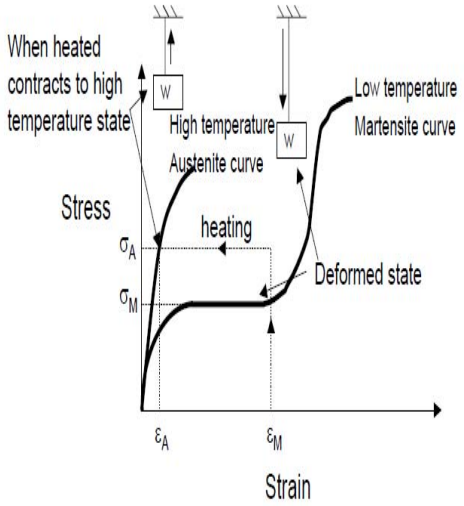

Figure 2: Stress-Strain Memory effects of an SMA wire

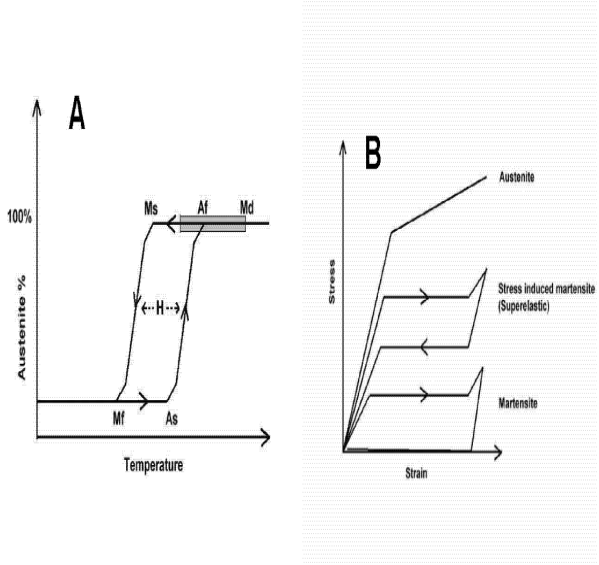

Figure 3: (A) Martensitic transformation and hysteresis (= H) upon a change of temperature. As = austenite start, Af = austenite finish, Ms = martensite start, Mf = martensite finish and Md = Highest temperature to strain-induced martensite. Gray area = area of optimal super elasticity, and (B) Stress-strain behaviour of different phases of NiTi at constant temperature.

A centrifugal pump is a device whose primary purpose is to produce pressure by accelerating fluid particles to high velocity providing them with velocity energy [ref 3] and one of the major parameters used to analyse the performance of a pump is the mass flow rate of fluid through the pump. For incompressible flow, it is more common to use Volume flow rate rather than mass flow rate [14, 15]. Manufacturers now develop a "smart" pump which incorporates microprocessors as part of their normal function [15]. A smart pumping system must be capable of knowing when to adjust itself to system changes without manual intervention. The system must also be fault tolerant.

The use of the one-way shape memory or superelastic property of NiTi for a specific application requires a piece of NiTi to be molded into the desired shape. The characteristic heat treatment is then done to set the specimen to its final shape. The heat treatment methods used to set shapes in both the shape memory and the superelastic forms of NiTi are similar. Adequate heat treatment parameters (temperature and suitable time) are needed to set the shape and the properties of the item [16]. They must usually be determined experimentally for the requirements of each desired part. Rapid cooling of some kind is preferred, such as water quenching or rapid fluid cooling. Certainly over the past few decades, significant progress has been made in the areas of pump hydraulics, mechanical design and applications through the use of computerized tools such as computational fluid dynamics (CFD) and finite element analysis (FEA). In this study, the shape memory effect exhibited by NiTi shape memory alloys will be utilized in the description of the Shape Memory Smart Impeller. It is thus believed that as the temperature of the fluid being pumped through the system is increased, the change in temperature will induce a phase transformation in the NiTi blade from Martensite to the parent phase, Austenite

II. Constitutive Modeling of NiTi Shape Memory Alloys

The Brinson model uses constant material functions and offers the advantage of capturing the thermo-mechanical behavior of SMA's at any temperature. The model introduces the stress-induced Es and the temperature-induced Et martensite volume fraction. Based on the energy balance law, the constitutive relation for SMA's according to the Brinson model [45] is given as:

$$\sigma - \sigma^0 = E(\xi)\varepsilon - E(\xi^0)\epsilon^0 + \Omega(\xi)\xi - \Omega(\xi^0)\xi^0 + \Theta(T - T^0) \quad (1)$$

where the quantities in the initial state is given by the suffix ^{0}, and the actual quantities without the suffix. E is the Young's modulus, and is given in terms of a linear function of the martensite phase as:

$$E = E_A + \xi(E_M + E_A) \quad (2)$$

with E_A and E_M representing the 100% austenite and 100% martensite Young's Moduli respectively. ξ represent the martensite phase fraction present in the material and is composed of two types, i.e. thermally transformed and stress induced, given as:

$$\xi = \xi_T + \xi_T \quad (3)$$

Ω represent transformation tensor, related to Young's Modulus, and is given in the form

$$\Omega(\xi) = -\varepsilon_{T_r} E(\xi) \quad (4)$$

ε_{T_r} is the maximum transformation strain and for this particular situation assumed to be related to the displacement, δ, of the curved beam.

The final term in equation 1, $\Theta(T - T^0)$ is related to the thermal strain generated in the SMA due to the rise in temperature and Θ is equivalent to the thermal expansion of the SMA.

Assuming the material is in its initial state it is free from stress, in a fully twinned martensite state, and the elastic strain components are negligible compared to the transformation strain, equation 1 is now dependant only on thermal and transformation strains and is reduced to

$$\sigma = \Omega(\xi)\xi + \Theta(T - T^0) \quad (5)$$

Assuming the transformation is not dependant on stress, Brinson [45] proposed the following relations associated ξ and T for equation 3.

For the conversion to Austenite

$$\xi_{M\to A} = \frac{\xi}{2}[COS[a_A(T - A_s)] + 1] \quad (6)$$

Where

$$a_A = \frac{\pi}{(A_f - A_s)} \quad (7)$$

When $T > A_s$

For the conversion to Martensite

$$\xi_{M\to A} = \frac{1-\xi}{2}[\cos[a_A(T - A_s)] + 1] \quad (8)$$

where

$$a_M = \frac{\pi}{(M_s - M_f)}$$

when $M_f < T < M_s$ and$T < T^0$, else $\xi_{M\to A} = 0$

For transformation to austenite, the total transformation displacement δ is further given as

$$\delta = \delta_A + \xi_{A\_M}(\delta_M - \delta_A) \quad (9)$$

for transformation to martensite

$$\delta = \delta_A + \xi_{M\_A}(\delta_M - \delta_A) \quad (10)$$

With

$$\delta = \sqrt{(\delta_X)^2 + (\delta_y)^2} \quad (11)$$

δ_A *and* δ_M represents the transformation deformation of each phase. The components of displacement δ_X *and* δ_y represent the horizontal and vertical movement at the free end of the curved SMA insert.

III.

Conceptualization and Structural Model of Shape Memory Smart Impeller

The NiTi strip is treated as a thin beam we find a possible solution to the operating mechanism of the Shape Memory Smart Impeller (see Fig. 4). At normal operating conditions, i.e. temperatures below A_s temperature, the NiTi thin beam assumes the inner shape of the impeller blade, The mechanism of actuation for our smart impeller is driven purely by thermal changes, i.e. increases in temperature from A_s to A_f will transform the twinned martensite to austenite, thus causing the shape change from a 30^0 inlet angle and 30^0 outlet angle to 30^0 inlet angle and 55^0 outlet angle. In the reverse transformation, i.e. a decrease in temperature from M_s to M_f, will transform the austenite back to twinned martensite and the SMA reverts back to the 30^0 inlet angle and 30^0 outlet angles. Any change in the fluid temperature to above A_s and A_f will result in the NiTi SMA transforming from its low temperature martensitic state to the high temperature austenitic state. The latter state would be set to conform to the blade angle for 30^0 inlet angle and 55^0 outlet angle.

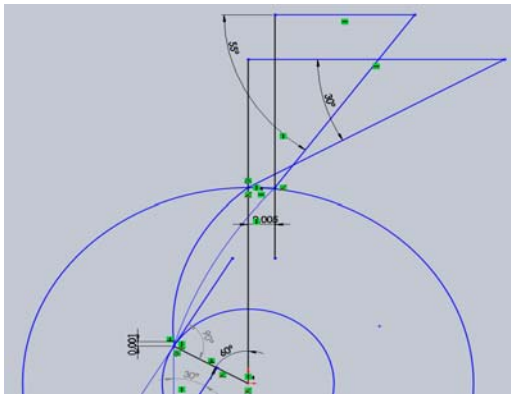

Figure 4: Operating mechanism of the Shape Memory Smart Impeller

Changing the centrifugal impeller blade outlet angle increases outlet velocity and in turn the pressure head, as well as the work done by the impeller on the fluid passing through the system. The impellers (see Figs 5 and 6) were designed to have their outside blade sections remain identical while the inside blade section changes as the blade outlet angle is increased. The fluid flow passage (horizontal measurement) is decreased as the outlet blade angle is increased .For impeller blade outlet angles 45, 50, and 55 degrees the percentage decrease in the horizontal measure of fluid flow passage was determined as 1.086, 10.15, and 12.71 respectively. if we consider the entire blade or a section of it to be constituted of NiTi shape memory alloys and utilizing the shape memory effect it will be possible to change the blade outlet angle if the temperature of the fluid is increased above the NiTi specific A_s transition temperature, thus decreasing the fluid flow passage and increasing outlet velocity, pressure and work done by the impeller on the fluid. The NiTi SMA will be in its softer martensitic phase under normal condition. Any increase in the temperature of the fluid will then lead to the thermo-elastic phase transformation from martensite to austenite. The NiTi SMA should thus be trained to transform to the predefined shape of the 55 degree blade outlet angle on heating and revert back to the 30 degree outlet angle upon cooling.

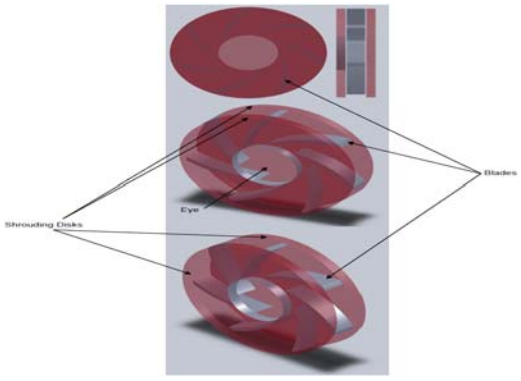

Figure 5: 3D Model of Centrifugal Pump Impeller showing blades, eye, shrouding disks

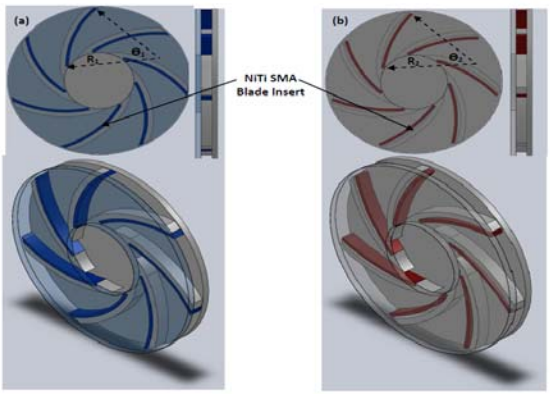

Figure 6: Idealized model of the Shape Memory Smart Impeller with (a) showing low temperature configuration and (b) showing high temperature configuration

Furthermore it assumed that the free end (see Fig. 4) moves within a guide until the final state is achieved. The shape memory effect exhibited by shape memory alloys will be utilized to affect actuation of the Shape Memory Smart Impeller. At normal operating conditions, i.e. fluid temperatures below austenite start temperature, the NiTi insert will conform to the shape of a blade with 30^0 inlet angle and 30^0 outlet angle. If the temperature of the water increases to above the austenite start temperature and continues to rise to austenite finish temperature thus fully transforming martensite to austenite, the NiTi insert will take the form of a blade with 30^0 inlet angle and 50^0 outlet angle. See Fig 7, the transformation strain is thus equal to the displacement (δ) of the curved beam. This shape change due to the temperature increase causes an internal stress to be developed in the NiTi insert equal to the circumferential stress.

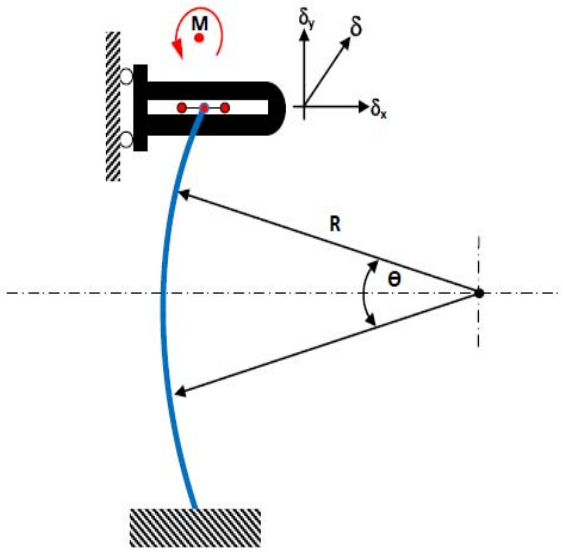

Figure 7: Idealized model of operating mechanism of the Shape Memory Smart Impeller

IV. Simulation Algorithm for Engineering Fluid Dynamics

EFD.Lab, a full-featured general purpose CAD-embedded with finite volume fluid flow and heat transfer simulation tool was used for simulation, a rectangular adaptive meshing was used to mesh. This pump has a stationary axial inlet (an eye), a pipe section with a central body of circular arc contour, which turns the flow by 90 degrees from the axial direction. Water flows through a centrifugal pump having a rotating impeller (see figure 8). At the inlet's exit the radial water flow is sucked by a rotating impeller, which has seven untwisted constant-thickness backswept blades. Each blade is cambered from 30 degrees at the impeller inlet of 16 mm radius to range of 0 to 90 degrees at the impeller exit of 42 mm radius, both with respect to the radial direction. While keeping all configurations the same, only the impeller outlet angle was increase for each in impeller by 5 degree. The inlet angle for all impeller was 30 degrees. These blades are confined between the impeller shrouding disks rotating with the same (as the blades) angular speed of 2000 rpm. Volume flow rate of 0.3 m^3/s normal to the inner face of the Cover in the absolute frame of reference and Outlet Environment Pressure of 101325 Pa for the Environment pressure at the radial outlet face are used as the inlet and outlet boundary conditions respectively

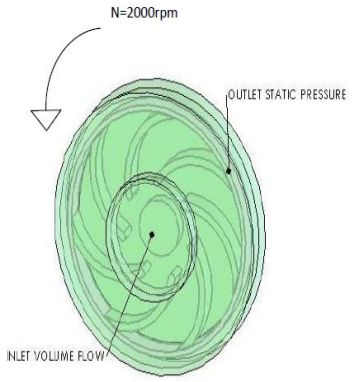

Figure 8: Centrifugal pumps with rotating impeller.

V. Results and Discussions

Considering the centrifugal pump impeller rotating at 1500rpm with inside and outside diameters of 100mm and 200mm respectively and fluid enters the impeller radially. The impeller blade inlet and outlet angles are 20^0 and 30^0 respectively. The work-done by the impeller on the fluid per unit weight of fluid was 17, 23 Nm/N. vary the impeller outlet blade angle from 5^0 to 90^0 with increments of 5^0 and holding all other terms constant. The outlet blade angle versus relative inlet velocity (for constant inlet angle of 20^0) is showing in Fig10. The outlet blade angle versus relative outlet velocity (for constant inlet angle of 20^0) is showed in fig 11 and the outlet blade angle versus Work-done (for constant inlet angle of 20^0) is in Fig 11. Form Figs. 9 – 11, it is clear shows that increases in the outlet angle (while keeping the inlet angle constant) will increase the relative inlet velocity, the relative outlet velocity, and Work-done on the fluid.

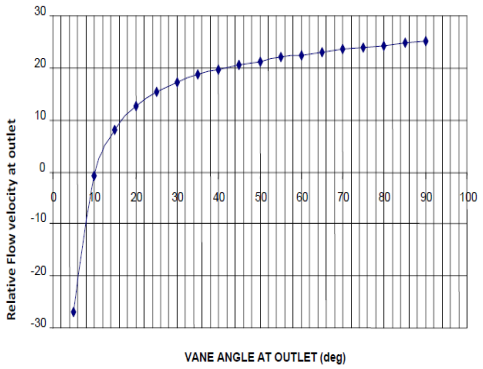

Figure: 9: A graph of Variable outlet angle versus relative flow velocity for a constant vane inlet angle of 20 degrees.

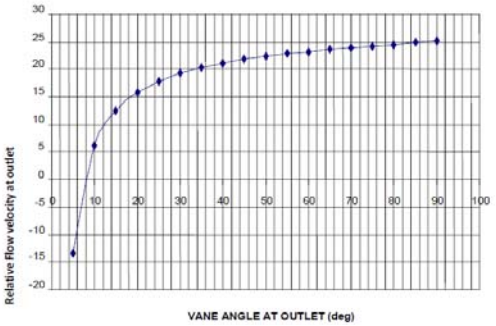

Figure 10: A graph of Variable outlet angle versus relative velocity at outlet for a constant vane inlet angle of 15 degrees.

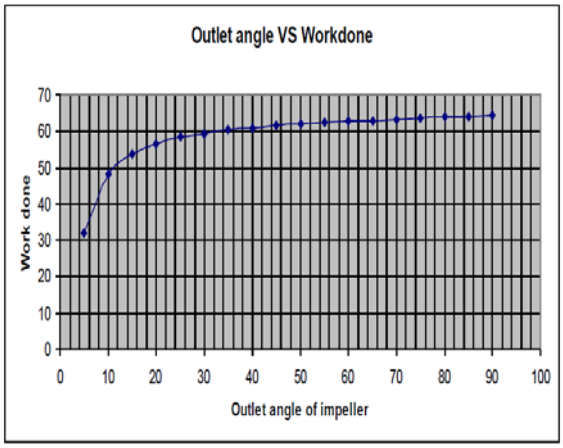

Figure 11: A graphs of Variable outlet angle versus work done for a constant vane inlet angle of 5 degrees.

From figure 12 using the 3D Solid Modeling software package, SolidWorks, to measured the middle of the inside blade to the center of rotation. For impeller blade outlet angles 45, 50, and 55 degrees the percentage decrease in the horizontal measure of fluid flow passage was determined as 1.086, 10.15, and 12.71 respectively. it is clear that the entire blade or a section of it to be constituted of NiTi shape memory alloys and utilizing the shape memory effect it will be possible to change the blade outlet angle if the temperature of the fluid is increased above the NiTi specific A_s transition temperature, thus decreasing the fluid flow passage and increasing outlet velocity, pressure and work done by the impeller on the fluid.

Considering the impeller, each having an inlet blade angle 30^0 but outlet angles varying from 30^0 to 55^0 with increments of 5^0. the velocity vectors and static pressure distribution are shown in fig. 13

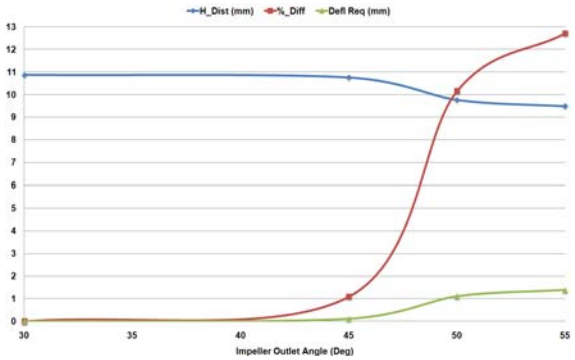

Figure 12: Dimensional Blade Angle Variations

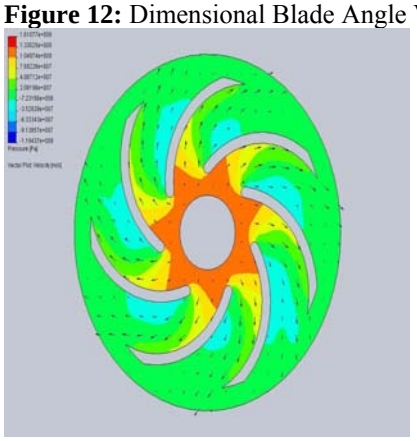

Figure 13: Pressure plot

From figure 14, it shows that the efficiency of the impeller drops drastically from 30 degrees inlet and 30 degrees outlet, but increases gradually as the outlet angle increase from this point. The graph also shows a characteristic optimum increase up to 45 degrees outlet where it starts to flatten out. This will allow us to have an angle of attack of 14 degrees from an inlet angle of 30 degrees. A Detail investigation reveals that there is a jump from 42 degrees to 45 degrees. Secondly there is a decrease from 45 degrees to 46 before increasing slowing onward. Investigating the torque on the system, it was revealed that despite an increase in the efficiency from 40 degrees to 42 degrees at the outlet, there is surprisingly a decrease in the torque in this section. See figure16. A closer look at the torque alone on both sides of 42 degrees (where there is a drop) confirms our V-shape (See Figure 16).

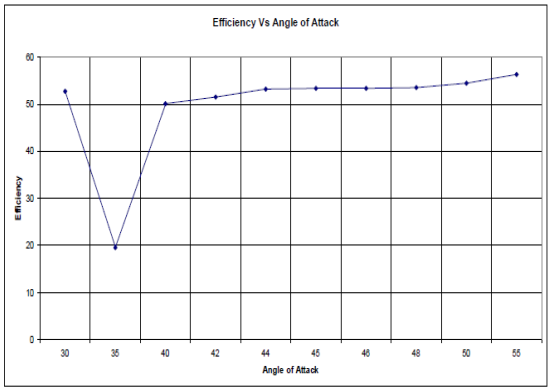

Figure 14: Detail investigation of efficiency versus angle of attack

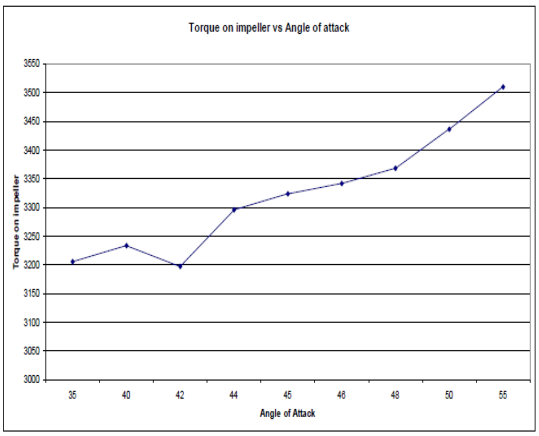

Figure 15: Detail investigation of impeller torque versus angle of attack.

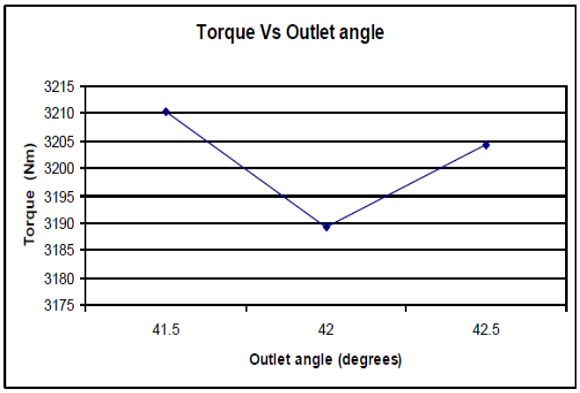

Figure 16: Torque vs. outlet angle

VI. Conclusion

This study successfully conceptualised a Shape Memory Smart Centrifugal Impeller that will increase fluid flow rate through a given system if the fluid temperature increases above a given transition temperature using NiTi Shape Memory Alloys was achieved .Based on the energy balance law, Brinson model was used to determine forward transformation, i.e. Martensite to Austenite, and the reverse transformation to describe the mechanism of operation of the Shape Memory Smart Impeller. The displacements change the outlet angle of the blade from 30^0 to 55^0.thus theoretically increasing the velocity at the outlet and increasing the head of the centrifugal impeller. For the computational fluid dynamics analyses, the results confirmed the optimum conditions of the specific system used to conceptualize the Shape Memory Smart Impeller. It also showed the formation of eddies, that would not typically be identified with the analytical solution. The benefits to for example the automotive industry would be the development of more efficient cooling systems. The operating benefits of such a pumping system include an increase in the cooling effect and higher efficiency thus providing less overheating, less impeller variation. Adaptability in adverse conditions and Ability to adjust itself to system changes without manual intervention

Acknowledgment

The authors would like to the National Research Foundation (NRF) and Faculty of Engineering and the Built Environment, Department of Mechanical Engineering Science, University of Johannesburg, Johannesburg, South Africa are acknowledged for the award of the research funds to support this study.

References

[1] V. Msomi, G. Oliver, O. Philander and K. Sanusi, "A Newly Developed Alternative Way to Describe Shape Memory Alloy Behaviour," in *International Conference on Computational Science and Its Applications*, Santander, Spain, 2011.

[2] W.Ochonski, "Application of shape memory materials in fluid sealing technology," *Industrial Lubrication and Tribology,* pp. 99 - 110, 2010.

[3] M. Braunovic, N. K. .. Myshkin and V. V. .. Konchits, "Fundamentals, Applications and Technology," in *Electrical Contacts*, CRC, 2006, pp. 565-583.

[4] G. Song, B. Kelly, B. Agrawal, P. Lam and T. Srivatsan, "Application of Shape Memory Alloy Wire Actuator for Precision Position Control of a Composite Beam," *Journal of Materials Engineering and Performance,* vol. 9, no. 3, pp. 330-333, 2000.

[5] G.Song, "Robust position regulation of a shape memory alloy wire actuator," *Journal of Intelligent Material Systems and Structures,* pp. 381-392, 2006.

[6] Y. Sung, G. Shan and L. Shen, "Fracture toughening mechanism of shape memory alloys under mixed-mode loading due to martensite transformation," *International Journal of Solids and Structures,* vol. 38, pp. 4463-4476, 2000.

[7] L. Petrini and F. Migliavacca, "Biomedical Applications of Shape Memory Alloys," *Journal of Metallurgy,* p. 15, 2011.

[8] X.Wang, Y.Bellouard and J. Vlassak, "Laser annealing of amorphous NiTi shape memory alloy thin films to locally induce shape memory properties," *Acta Materialia,* p. 4955–4961, 2005.

[9] J. A. Shaw, "A thermomechanical model for a 1-D shape memory alloy," *International Journal of Solids and Structures,* p. 1275–1305, 2002.

[10] J.A.Shaw and S.Kyriakides, "On the nucleation and propagation of phase transformation fronts in a NiTi alloy," *Acta Materialia,* vol. 45, no. 2, pp. 673-700, 1997.

[11] S.Nemat-Nasser and W.G.Guo, "Superelastic and cyclic response of NiTi SMA at various strain rates and temperatures," *Mechanics of Materials,* vol. 38, p. 463–474, 2006.

[12] G. Song, N. Maa and H.-N. Lib, "Applications of shape memory alloys in civil structures," *Engineering Structures,* vol. 28, p. 1266–1274, 2006.

[13] Y.Zhao, M.Taya, Y.Kang and A.Kawasaki, "A Compression behavior of porous NiTi shape memory alloy," *Acta Materialia,* vol. 53, p. 337–343, 2005.

[14] S. Bansal, "Solid and Fluid Mechanics," New Delhi, Laxmi Publications, 2007, pp. 322-490.

[15] P.E.Stavale, "Smart Pumping System: The Time Is Now," ITT Industries, Fluid Technology Corporation, Seneca Falls, NY USA, 2007.

[16] K. Otsuka and X. Ren, "Physical metallurgy of Ti-Ni-based shape memory alloys," *Progress in Materials Science,* vol. 50, no. 5, p. 511–678, 2005.

[17] L. C. Brinson, "One-dimensional constitutive behavior of shape memory alloys: thermomechanical derivation with non-constant material functions and redefined martensite internal variable," *Journal of Intelligent Material Systems and Structures,* vol. 4, no. 2, p. 229–242, 1993.